Hindawi Publishing Corporation
Journal of Biomedicine and Biotechnology
Volume 2012, Article ID 848042, 10 pages
doi:10.1155/2012/848042

Research Article

Identification of HLA-A24-Restricted Novel T Cell Epitope Peptides Derived from P-Cadherin and Kinesin Family Member 20A

Ryuji Osawa,[1,2] Takuya Tsunoda,[1,2,3] Sachiko Yoshimura,[1,2] Tomohisa Watanabe,[2] Motoki Miyazawa,[1] Masaji Tani,[1] Kazuyoshi Takeda,[4] Hidewaki Nakagawa,[3] Yusuke Nakamura,[3] and Hiroki Yamaue[1]

[1] *Second Department of Surgery, Wakayama Medical University, 811-1 Kimiidera, Wakayama 641-8510, Japan*
[2] *OncoTherapy Science Inc. Research Department, Kanagawa 213-0012, Japan*
[3] *Laboratory of Molecular Medicine, Human Genome Center, Institute of Medical Science, The University of Tokyo, Tokyo 108-8639, Japan*
[4] *Department of Immunology, Juntendo University School of Medicine, Tokyo 113-8421, Japan*

Correspondence should be addressed to Hiroki Yamaue, yamaue-h@wakayama-med.ac.jp

Received 6 February 2012; Revised 9 April 2012; Accepted 9 April 2012

Academic Editor: Soldano Ferrone

Copyright © 2012 Ryuji Osawa et al. This is an open access article distributed under the Creative Commons Attribution License, which permits unrestricted use, distribution, and reproduction in any medium, provided the original work is properly cited.

We here identified human leukocyte antigen-(HLA-)A*2402-restricted epitope peptides from Cadherin 3, type 1, P-cadherin (CDH3) and kinesin family member 20A (KIF20A) that were found to be specifically expressed in cancer cells through genome-wide expression profile analysis. CDH3-10-807 peptide and KIF20A-10-66 peptide successfully induced specific CTL clones, and these selectively responded to COS7 cells expressing both HLA-A*2402 and respective protein while did not respond to parental cells or COS7 cells expressing either HLA-A*2402 or respective protein. Furthermore, CTL clones responded to cancer cells that endogenously express HLA-A*2402 and respective protein, suggesting that CDH3-10-807 peptide and KIF20A-10-66 peptide are naturally presented on HLA-A*2402 molecule of human cancer cells. Our results demonstrated that CDH3-10-807 peptide and KIF20A-10-66 peptide are novel HLA-A24-restricted tumor-associated antigens and would be applicable for CTL-inducing cancer therapies.

1. Introduction

After identification of the melanoma antigen gene (MAGE) family as a tumor-associated antigen (TAA), a number of TAAs have been revealed by means of various approaches including SEREX and cDNA library screening [1–6]. Some TAAs, such as MAGE, gp100, and MUC1, have been applied to treat various cancers in clinical trials [7–9], and vaccine-based therapy is now considered as a promising approach to fight against various cancers [10–13].

We have identified dozens of genes specifically expressed in cancer cells by genome-wide expression profile analysis for cDNA microarray consisting of more than 30,000 cDNAs and expressed sequence tags (ESTs) [14]. Among them, two genes, Cadherin 3, type 1, P-cadherin (CDH3) and kinesin family member 20A (KIF20A), were found to be upregulated in pancreatic cancers [15, 16]. CDH3 is one of the classic cadherin family that plays a critical role in cell-cell adhesion and epithelial morphogenesis [17]. We reported that over-expression of CDH3 promoted the motility of cancer cells and blocking of CDH3 by anti-CDH3 antibody inhibited the migration of CDH3-expressing cells [15]. KIF20A is a member of the kinesin family, which is characterized to be a motor protein in cancer cells [18], and northern analysis indicated no expression of KIF20A among examined 23 normal tissues except testis. Furthermore, knock down of KIF20A expression with small interfering RNA suppressed the proliferation of pancreatic ductal adenocarcinoma cells [16].

Thus, both CDH3 and KIF20A would play oncogenic functions in pancreatic cancer cells and are attractive target molecules for cancer therapies including immunotherapy.

We here identified CDH3- and KIF20A-derived novel HLA-A*2402-restricted epitope peptides that can induce peptide-specific cytotoxic T lymphocyte (CTL), suggesting that these epitope peptide would be applicable to peptide-based cancer vaccine therapies for HLA-A*2402 positive pancreatic cancer patients.

2. Materials and Methods

2.1. Peptides. CDH3 and KIF20A-derived 9-mer and 10-mer peptides that have high binding affinity (binding score > 10) to HLA-A*2402 were predicted by the binding prediction software "BIMAS" (http://www-bimas.cit.nih.gov/molbio/hla_bind/) and were synthesized by Sigma-Aldrich Japan KK (Ishikari, Japan) according to a standard solid-phase synthesis method and purified by reversed-phase high-performance liquid chromatography (HPLC). HIV-A24 epitope peptide (RYLRDQQLL) [19] was also synthesized as a negative control. The purity (>90%) and the identity of the peptides were confirmed by analytical HPLC and mass spectrometry analysis, respectively. Peptides were dissolved in dimethylsulfoxide at 20 mg/mL and stored at −80°C.

2.2. Cell Lines. CDH3- and KIF20A- negative Human B-lymphoblastoid cell line TISI (HLA-A*2402) was purchased from the IHWG Cell and Gene Bank (Seattle, WA). Monkey kidney cell line COS7, human B-lymphoblastoid cell line Jiyoye (HLA-A32), human B-lymphoblastoid cell line EB-3 (HLA-A3/Aw32), and CDH3-expressing human lung cancer cell line H358 (HLA-A3) were purchased from American Type Culture Collection (Manassas, VA). CDH3-expressing human pancreatic cancer cell line PK-45P (HLA-A24/A33) and KIF20A-expressing human pancreatic cancer cell line PK-59 (HLA-A31/A33) were provided by Cell Resource Center for Biomedical Research, Tohoku University (Sendai, Japan). KIF20A-expressing human stomach cancer cell line MKN-45 (HLA-A24) and MiaPaCa-2 cells (HLA-A24) were purchased from Health Science Research Resources Bank (Osaka, Japan). TISI, Jiyoye, EB-3, H358, PK-45P, PK-59, and MKN-45 were maintained in RPMI1640 media (Invitrogen, Carlsbad, CA), COS7 were maintained in DMEM media (Invitrogen), and MiaPaCa-2 cells were maintained in EMEM media (Invitrogen). Each medium was supplemented with 10% fetal bovine serum (GEMINI Bio-Products, West Sacramento, CA) and 1% antibiotic solution (Sigma-Aldrich, ST. Louis, MO). The expression of CDH3 and KIF20A protein was confirmed by Western blotting using anti-CDH3 antibody (BD Transduction Labs., BD Biosciences, San Jose, CA) or anti-KIF20A antibody (Bethyl Laboratories, Montgomery, TX).

2.3. In Vitro Induction of Peptide-Specific CTL. To examine the ability to induce peptide-specific CTL, purified $CD8^+$ T cells were cocultured with autologous monocyte-derived mature dendritic cells (DCs) pulsed with peptide. Both $CD8^+$ T cells and DCs were prepared from peripheral blood mononuclear cells (PBMCs) of same HLA-A*2402-positive healthy volunteers. Briefly, PBMCs were isolated by Ficoll-Paque solution (GE Healthcare, Uppsala, Sweden), then cells were cultured in AIM-V medium (Invitrogen) containing 2% heat-inactivated autologous serum (AS). After the over night incubation, nonadherent cells were washed out, then 1000 U/mL of granulocyte-macrophage colony-stimulating factor (GM-CSF; R&D Systems, Minneapolis, MN) and 1000 U/mL of interleukin (IL)-4 (R&D Systems) were added in the culture to induce monocyte-derived DCs. To mature DCs, 0.1 KE/mL of OK-432 (Chugai Pharmaceutical Co., Tokyo, Japan) was added in the culture on day 5. Seven days later, DCs were pulsed with 20 μg/mL of synthesized peptide in AIM-V medium containing 3 μg/mL of β2-microglobulin (Sigma-Aldrich) at 37°C for 3 h [20] and incubated in the media containing 30 μg/mL of Mitomycin C (MMC) (Kyowa Hakko Kirin Co. Ltd., Tokyo, Japan) for 30 min. Following washing out residual peptide and MMC, cells were used as antigen-presenting cells to induce peptide-specific CTL. Generated monocyte-derived mature DCs expressed CD80, CD83, CD86, and HLA class II on their cell surface (data not shown). Autologous $CD8^+$ T cells were prepared from PBMCs derived from the same HLA-A*2402-positive donor by positive selection with Dynal CD8 positive isolation kit (Invitrogen) according to the manufacturer's instructions. 1.5×10^4 of peptide-pulsed DCs and 3×10^5 of $CD8^+$ T cells were cocultured in 0.5 mL of AIM-V medium supplemented with 10 ng/mL of IL-7 (R&D Systems) and 2% AS on 48-well plates (Corning Inc., Corning, CA). IL-2 (CHIRON, Emeryville, CA) was added to the culture at 20 IU/mL 3 days after coculture, and peptide-pulsed DCs were additionally supplied into the culture on days 7 and 14. Eight wells were prepared for CTL induction by every peptide in a single experiment. On day 21, interferon- (IFN-) γ production was examined by IFN-γ enzyme-linked immunospot (ELISPOT) assay under the stimulation with peptide-pulsed TISI cells.

2.4. IFN-γ Enzyme-Linked Immunospot (ELISPOT) Assay. T cell response to epitope peptide was measured by ELISPOT assay using IFN-γ ELISPOT kit and AEC substrate set (BD Pharmingen, San Diego, CA) according to the manufacturer's instruction. Briefly, TISI cells were pulsed with 20 μg/mL of respective peptide at 37°C for 20 h, and the residual peptide that did not bind to TISI cells was washed out to prepare peptide-pulsed TISI cells as the stimulator cells. 200 μL of cell culture suspension were distributed to two wells (100 μL each) on Multiscreen-IP 96-well plate (Millipore, Bedford, MA) following removing 500 μL of supernatant from each well from culture of "*in vitro* induction of peptide-specific CTL." Cells were co-incubated with peptide-pulsed TISI cells (1×10^4 cells/well) at 37°C for 20 h. The plates were analyzed by the automated ELISPOT reader, ImmunoSPOT S4 (Cellular Technology Ltd, Cleveland, OH) and ImmunoSpot Professional Software Version 5.0 (Cellular Technology Ltd). TISI cells pulsed with HIV-A24 epitope peptide (RYLRQQLLGI) were used as control. When the spot number in the peptide-stimulating

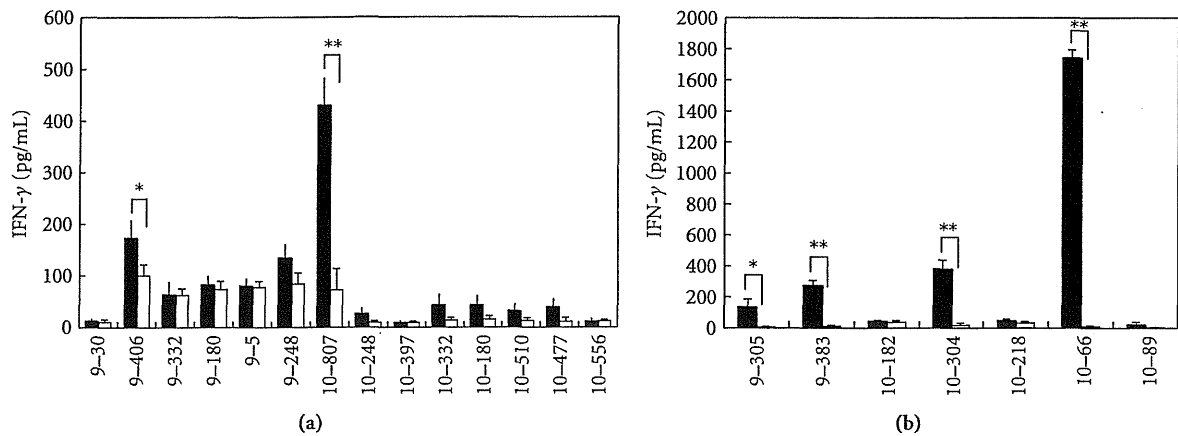

FIGURE 1: IFN-γ production from CTLs responding to CDH3- or KIF20A-derived peptides. IFN-γ production by CTLs induced with CDH3-derived peptides (a) or KIF20A-derived peptides (b) responding to respective peptide-pulsed HLA-A*2402 positive TISI cells. CTLs were expanded and harvested following "*in vitro* induction of peptide-specific CTL," and IFN-γ production was examined by IFN-γ ELISA. "Closed bar" indicates the mean IFN-γ production responding to TISI cells pulsed with indicated peptide, and "open bar" indicates the mean IFN-γ production responding to TISI cells pulsed with HIV-A24 peptide (negative control). All experiments were performed triplicate. Similar results were obtained in three to five independent experiments. $^{*}P < 0.05$, $^{**}P < 0.01$.

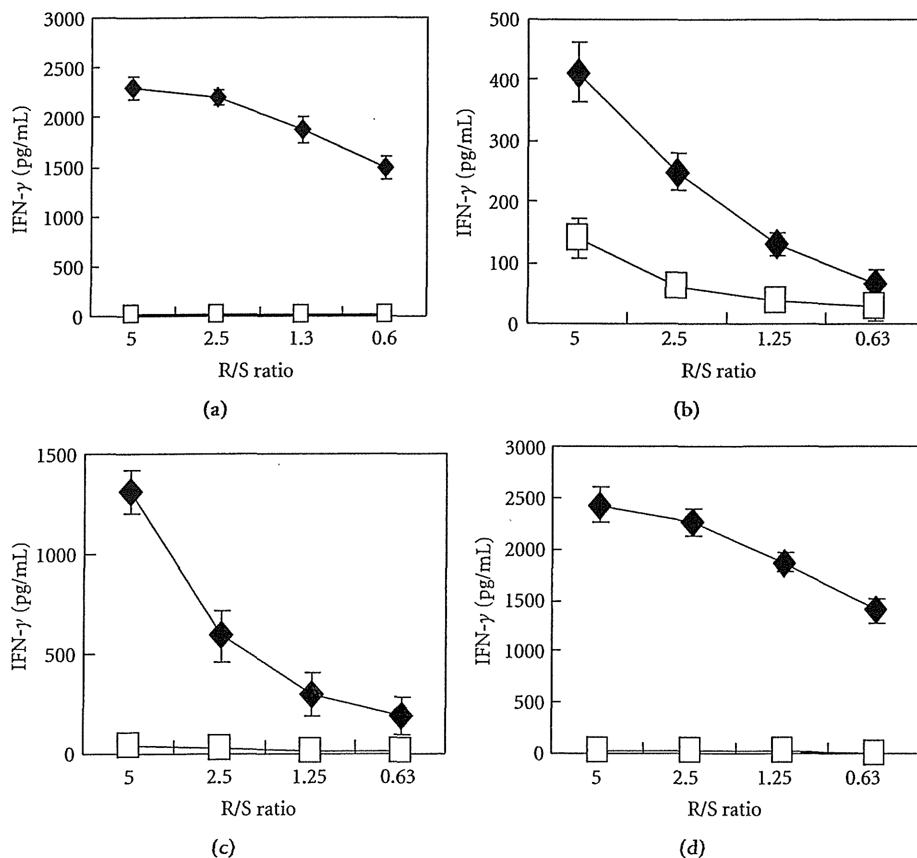

FIGURE 2: Peptide-specific IFN-γ production by CTL clones. IFN-γ production by CDH3-10-807 peptide-specific CTL clone (a), KIF20A-9-305 peptide-specific CTL clone (b), KIF20A-10-304 peptide-specific CTL clone (c), and KIF20A-10-66 peptide-specific CTL clone (d), when stimulated with TISI cell pulsed with corresponding peptide (closed diamond) or HIV-A24 peptide (open square). CTL clones produced significant amount of IFN-γ responding to corresponding peptide. IFN-γ ELISA was performed triplicate. R/S ratio, responder cell (CTL clone)/stimulator cell (TISI cell) ratio.

Table 1: Candidates of epitope peptide derived from CDH3 and KIF20A.

CDH3				KIF20A			
Start position	Amino acid sequence (mer)	Binding score	CTL induction	Start position	Amino acid sequence (mer)	Binding score	CTL induction
513	IYEVMVLAM (9)	37.5	–	308	IYNELLYDL (9)	432	–
667	LFLLLVLLL (9)	36	–	621	MYEEKLNIL (9)	432	–
30	VFREAEVTL (9)	24	+	67	VYLRVRPLL (9)	420	–
406	LYVEVTNEA (9)	16.6	+	499	KFSAIASQL (9)	56	–
332	KYEAHVPEN (9)	16.5	+	304	SFFEIYNEL (9)	44.352	–
180	KYELFGHAV (9)	15	+	187	IFNSLQGQL (9)	36	–
85	RSLKERNPL (9)	14.4	–	305	FFEIYNELL (9)	30	+
5	RGPLASLLL (9)	12	+	23	MFESTAADL (9)	30	–
652	KGGFILPVL (9)	11.2	–	256	SFDSGIAGL (9)	20	–
248	TYNGVVAYS (9)	10.5	+	298	RFSIWISFF (9)	20	–
65	LFSTDNDDF (9)	10	–	383	IFSIRILHL (9)	20	+
807	DYLNEWGSRF (10)	150	+	647	KIEELEALL (9)	17.28	–
248	TYNGVVAYSI (10)	105	+	625	KLNILKESL (9)	14.4	–
667	LFLLLVLLLL (10)	42	–	695	KLQQCKAEL (9)	13.2	–
397	DFEAKNQHTL (10)	30	+	726	FTIDVDKKL (9)	11.088	–
332	KYEAHVPENA (10)	21	+	688	QLQEVKAKL (9)	11.088	–
180	KYELFGHAVS (10)	15	+	308	IYNELLYDLL (10)	432	–
510	RNNIYEVMVL (10)	12	+	182	RSLALIFNSL (10)	24.192	+
5	RGPLASLLLL (10)	12	–	304	SFFEIYNELL (10)	24	+
477	RILRDPAGWL (10)	12	+	742	RLLRTELQKL (10)	15.84	–
556	CNQSPVRQVL (10)	10.1	+	739	KNIRLLRTEL (10)	15.84	–
				218	RQEEMKKLSL (10)	14.4	+
				70	RVRPLLPSEL (10)	12.672	–
				871	RILRSRRSPL (10)	12	–
				89	RIENVETLVL (10)	12	+
				364	KNQSFASTHL (10)	12	–
				66	KVYLRVRPLL (10)	11.2	+
				60	DSMEKVKVYL (10)	10.08	–

Start position indicated the number of amino acids from the N terminal of CDH3 and KIF20A.
Binding score was obtained using BIMAS program.
CTL induction was indicated as positive (+) or negative (–). Similar results were obtained 3–7 independent experiments using PBMC of 3–7 healthy volunteers.

well was more than 50 spots/well compared with that in the control well, we estimated that peptide-specific CTL were induced (positive) and subsequently expanded CTL from the positive well. Sensitivity of our ELISPOT assay was estimated as approximately average level by ELISPOT panel of Cancer Immunotherapy Consortium [CIC (http://www.cancerresearch.org/consortium/assay-panels/)].

2.5. CTL Expansion. Peptide-specific CTL obtained from CTL positive well of "*in vitro* induction of peptide-specific CTL" were expanded by the modified protocol based on the previously described methods [21–24]. Briefly, 5×10^5 of CTLs were cocultured with 5×10^6 of MMC-treated (30 μg/mL at 37°C for 30 min) EB-3 and Jiyoye cells in 25 mL of AIM-V containing 5% AS and 40 ng/mL of anti-CD3 mAb. The cultures were supplemented with IL-2 (final concentration: 120 IU/mL) 24 h later and fed with AIM-V medium containing 5% AS and IL-2 (30 IU/mL) on day 5, 8, and 11. On day 14, expanded T cells were harvested to examine specific response to epitope peptide by IFN-γ enzyme-linked immunosorbent assay (ELISA).

2.6. Establishment of Peptide-Specific CTL Clone. Peptide-specific CTL clones were established by limiting dilution method from the expanded CTLs specifically responding to epitope peptide. Briefly, T cells were diluted to 0.3, 1, and 3 cells/well in 96-well round-bottomed plates and cultured with 1×10^4 cells/well of MMC-treated EB-3 and Jiyoye cells in 150 μL of AIM-V containing 5% AS, 125 IU/mL of IL-2, and 30 ng/mL of anti-CD3 mAb. The culture was supplemented with IL-2 to the final concentration of 125 IU/mL on day 10. On day 14, IFN-γ production from peptide-specific CTL clones was examined by IFN-γ ELISA. Some peptide-specific CTL clones were expanded as described above.

2.7. IFN-γ ELISA. In some experiments, established CTLs were co-incubated with 1×10^4 cells of respective peptide-pulsed TISI cells or 5×10^4 cells of COS7 cells in 200 μL of AIM-V/5% AS media on 96-well round bottom plate (Corning Inc.). After 24 h incubation, cell free supernatants were harvested and IFN-γ production was examined by human

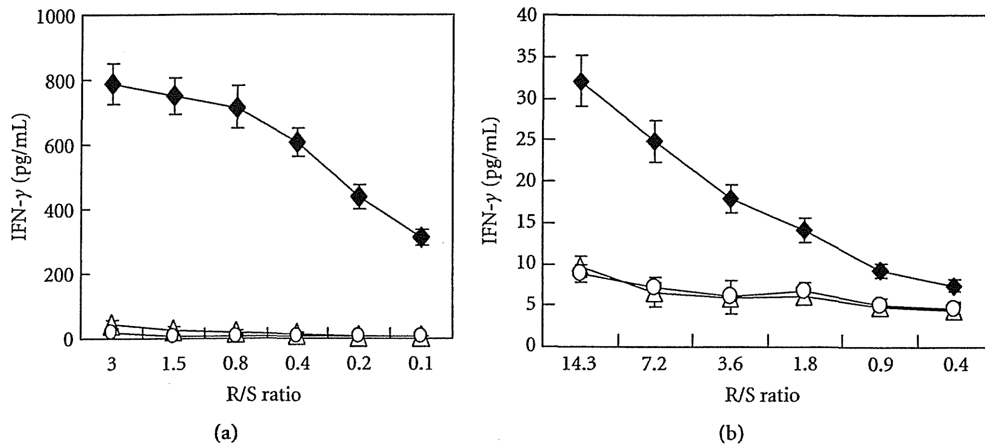

FIGURE 3: IFN-γ production by CTL clones responding to COS7 cells that expressing HLA-A*2402 and respective oncogene. (a) IFN-γ production by CDH3-10-807 peptide-specific CTL clone when exposed with COS7 cells expressing both HLA-A*2402 and CDH3 (closed diamond), HLA-A*2402 (open triangle), or CDH3 (open circle). (b) IFN-γ production by KIF20A-10-66 peptide-specific CTL clone when exposed with COS7 cells expressing HLA-A*2402 and KIF20A (closed diamond), HLA-A*2402 (open triangle), or KIF20A (open circle). Both CTL clones significantly produced IFN-γ responding to COS7 cells expressing HLA-A*2402 and corresponding gene. Similar results were obtained in three independent experiments. Independently induced other CTL clones also produced significant amount of IFN-γ when exposed with COS7 cell expressing both HLA-A*2402 and respective gene (data not shown). R/S ratio, responder cell (CTL clone)/stimulator cell (COS7 cell) ratio.

IFN-γ-specific ELISA kit (BD Pharmingen) according to the manufacturer's instructions.

2.8. Cytotoxicity Assay. Specific cytotoxic activity of induced CTL clones was tested by a 4 h ^{51}Cr release assay as previously described [25]. Data are represented as the mean ± SD of triplicate samples.

2.9. Transfection of HLA-A24 and/or Oncogene (CDH3 or KIF20A). HLA-A*2402 coding region was obtained from TISI cells. The cDNA encoding an open reading frame of HLA-A*2402 gene with FLAG tag or oncogene (CDH3 or KIF20A) coding region with the Myc tag sequence was amplified with PCR and cloned into pcDNA3.1 vector (Invitrogen). COS7 cells transiently expressing HLA-A*2402 and/or oncogene were prepared by the transfection of the vectors encoding respective genes using lipofectamine 2000 (Invitrogen) according to the manufacturer's instruction. The expression of HLA-A*2402 and oncogene-derived protein was confirmed by Western blotting using anti-Myc (Upstate Biotechnology, Lake Placid, NY) or anti-FLAG antibody (Sigma-Aldrich). Two days after transfection, the transfected cells were harvested with versene (Invitrogen) and used to stimulate peptide-specific CTL clones. IFN-γ production by CTLs was examined by IFN-γ-specific ELISA.

2.10. Flow Cytometry. Expression of peptide-specific T cell receptor (TCR) was examined on FACS-CantoII (Becton Dickinson, San Jose, CA) using peptide-HLA-A*2402 dextramer-PE (Immudex, Copenhagen, Denmark) (CDH3-10-807/MHC-dextramer-PE and KIF20A-10-66/MHC-dextramer-PE) according to the manufacturer's instructions. HIV-A24 epitope peptide (RYLRDQQLL)/MHC-dextramer was used as negative control. Briefly, expanded CTL lines were incubated with peptide-HLA-A*2402 dextramer-PE for 10 minutes at room temperature, then treated with FITC-conjugated anti-human CD8 mAb, APC-conjugated anti-human CD3 mAb, PE-Cy7-conjugated anti-human CD4 mAb, and 7-AAD (BD Pharmingen) at 4°C for 20 minutes.

3. Results

*3.1. Induction of CTL Responding to CDH3- or KIF20A-Derived Peptide Restricted with HLA-A*2402.* Based on the analysis with the binding prediction software "BIMAS," we synthesized 21 CDH3-derived epitope-peptides and 28 KIF20A-derived epitope-peptides that were expected to have high affinity to HLA-A*2402 molecule and activate CTLs (Table 1).

HLA-A*2402-positive CD8$^+$ T cells were cocultured with autologous DCs pulsed with respective peptide, and then peptide-specific IFN-γ production was analyzed by ELISPOT. Fourteen peptides derived from CDH3 and 7 peptides derived from KIF20A were able to induce peptide-specific CTLs producing IFN-γ (Table 1). Amongst these peptides, we successfully obtained CTLs that specifically produced significant amount of IFN-γ after CTL expansion when CDH3-9-406, CDH3-10-807, KIF20A-9-305, KIF20A-9-383, KIF20A-10-304, and KIF20A-10-66 peptide were pulsed (Figures 1(a) and 1(b)).

3.2. Establishment of CDH3- or KIF20A-Derived Peptide-Specific CTL Clones. Subsequently, we attempted to establish CTL clones by a limiting dilution. CDH3-10-807-, KIF20A-9-305-, KIF20A-10-304-, or KIF20A-10-66-specific CTL clones were established and produced a potent amount of

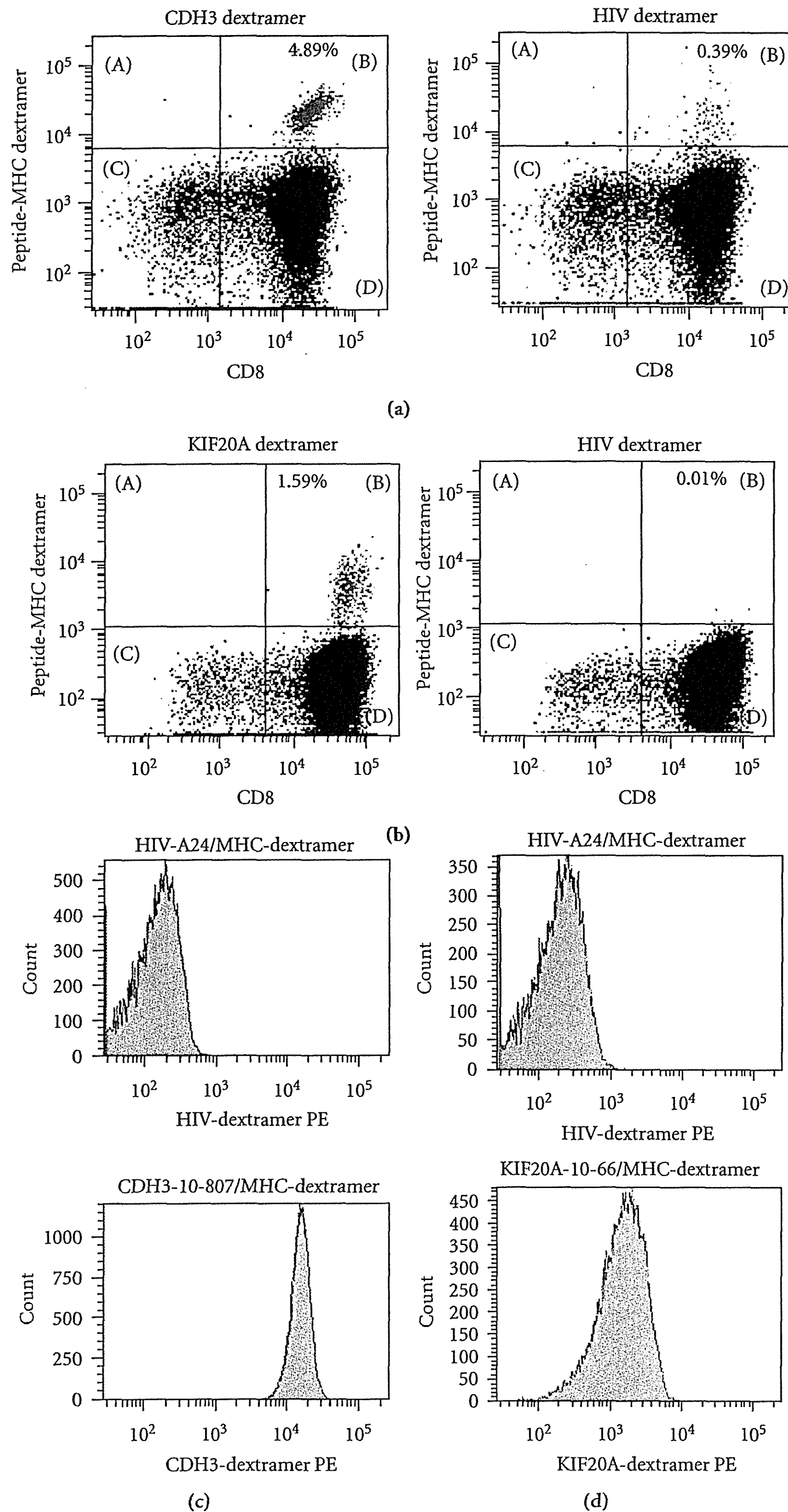

Figure 4: Peptide-specific TCR expression on CTL clones. (a) CDH3-10-807/HLA-A*2402-specific TCR expressing cells in expanded CTLs following "*in vitro* induction of peptide-specific CTL." (b) KIF20A-10-66/HLA-A*2402-specific TCR expressing cells in expanded CTLs following "*in vitro* induction of peptide-specific CTL." Results staining with anti-human CD8 mAb and CDH3-10-807/MHC-dextramer-PE or KIF20A-10-66/MHC-dextramer-PE are presented following gating on CD3-positive cells (left panels). Results staining with anti-human CD8 mAb and HIV-A24/MHC-dextramer-PE are presented as negative control following gating on CD3 positive cells (right panels). (c) CDH3-10-807/HLA-A*2402-specific TCR expression on CDH3-10-807-specific CTL clone. (d) KIF20A-10-66/HLA-A*2402-specific TCR expression on KIF20A-10-66-specific CTL clone. Staining with HIV-A24/MHC-dextramer-PE was used as negative control. CTL clones were $CD3^+$ and $CD8^+$ as expected (data not shown). Similar results were obtained in independent all experiments to examine CTL induction.

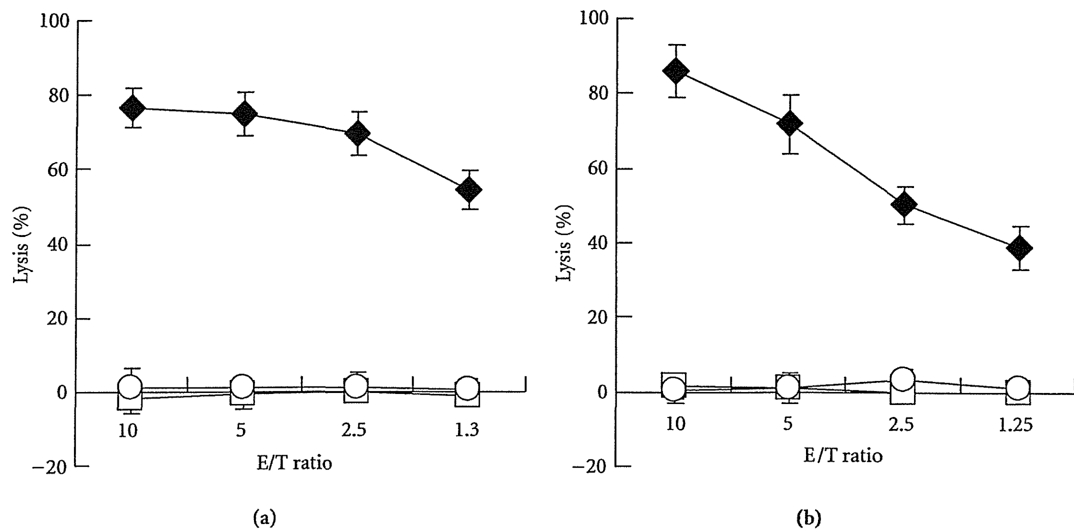

FIGURE 5: Cytotoxic activity of CTL clones against peptide-pulsed TISI cells. Cytotoxic activity of CDH3-10-807 peptide-specific CTL clone (a) and KIF20A-10-66 peptide-specific CTL clone (b) against HLA-A*2402-positive TISI cells pulsed with respective peptide (close diamond), HIV-A24 peptide (open square), or TISI cells without peptide pulse (open circle). E/T ratio, effector cell (CTL clone)/target cell (TISI cell) ratio. Similar results were obtained in three independent experiments using same CTL clone and in independent experiments using other CTL clones.

IFN-γ specifically responding to the stimulator cells pulsed with the respective peptide, but not HIV-A24 peptide (Figures 2(a)–2(d)).

*3.3. Recognition of Cells Endogenously Expressing Both HLA-A*2402 and Respective Protein by Peptide-Specific CTL Clones.* We then examined that the established peptide-specific CTL clones can recognize cells that express HLA-A*2402 and the target proteins. COS7 cells were transfected with plasmid designed to express HLA-A*2402 molecule and/or that to express the full length protein of CDH3 or KIF20A. We confirmed expression of these proteins by western blotting (data not shown). CDH3-10-807 peptide responding CTL clone substantially produced IFN-γ when exposed to COS7 cells that expressing both HLA-A*2402 and CDH3, but not COS7 cells that expressing either HLA-A*2402 or CDH3 (Figure 3(a)). Similarly, KIF20A-10-66 peptide responding CTL clone produced significant amount of IFN-γ when exposed to COS7 cells that expressing both HLA-A*2402 and KIF20A, but not COS7 cells that expressing either HLA-A*2402 or KIF20A (Figure 3(b)). Both CTL clones also produced IFN-γ responding to COS7 cells, which transfected with pIRES-vector containing both HLA-A*2402 and respective oncogene (data not shown). On the other hand, CTL clones responding to KIF20A-9-305 peptide or KIF20A-10-304 peptide did not produce IFN-γ when exposed to COS7 cells expressing both HLA-A*2402 and KIF20A (data not shown). Only CDH3-10-807 peptide and KIF20A-10-66 peptide, but not other candidate peptides, were able to induce CTL responding to COS7 cells expressing HLA-A*2402 and CDH3 or KIF20A, albeit we have tried several times using PBMC derived from different healthy donors (data not shown).

3.4. Peptide-Specific T Cell Receptor Expression. Expression of CDH3-10-807/HLA-A*2402- or KIF20A-10-66/HLA-A*2402-specific T cell receptor (TCR) was examined using CDH3-10-807/MHC-dextramer-PE or KIF20A-10-66/MHC-dextramer-PE. Significant population of $CD3^+$ $CD8^+$ cells, but not $CD3^+$ $CD8^-$ cells, expressed CDH3-10-807/HLA-A*2402- or KIF20A-10-66/HLA-A*2402- specific TCR after expansion of cells obtained by "*in vitro* induction of peptide-specific CTL" (Figures 4(a) and 4(b)). As expected, CTL clones established by CDH3-10-807 peptide- or KIF20A-10-66 peptide-pulsed cells were CD8 positive and expressed respective peptide/HLA-A*2402-specific TCR (Figures 4(c) and 4(d)).

3.5. Cytotoxic Activity of CTLs. We also examined cytotoxic activity of CTL clones. CDH3-10-807 or KIF20A-10-66 peptide-specific CTL clone demonstrated cytotoxic activity against HLA-A*2402-positive TISI cells when respective peptide was pulsed, but not when HIV-A24 peptide was pulsed or peptide was not pulsed (Figures 5(a) and 5(b)). These results suggested that CDH3-10-807 or KIF20A-10-66 peptide-specific CTL clone specifically exerted cytotoxic activity responding to respective epitope peptide binding to HLA-A*2402 on cells.

We, then, finally examined the cytotoxic activity against cancer cells, which endogenously expressed CDH3 or KIF20A gene. Expression of CDH3 protein was confirmed in HLA-A*2402-positive PK-45P cells and HLA-A*2402-negative H358 cells, but HLA-A*2402-positive MiaPaca-2 cells did not express CDH3 (Figure 6(a)). CDH3-10-807 peptide-specific CTL clone exerted significant cytotoxic activity against CDH3-expressing HLA-A*2402-positive PK-45P cells, but not H358 or MiaPaca-2 cells (Figure 6(b)).

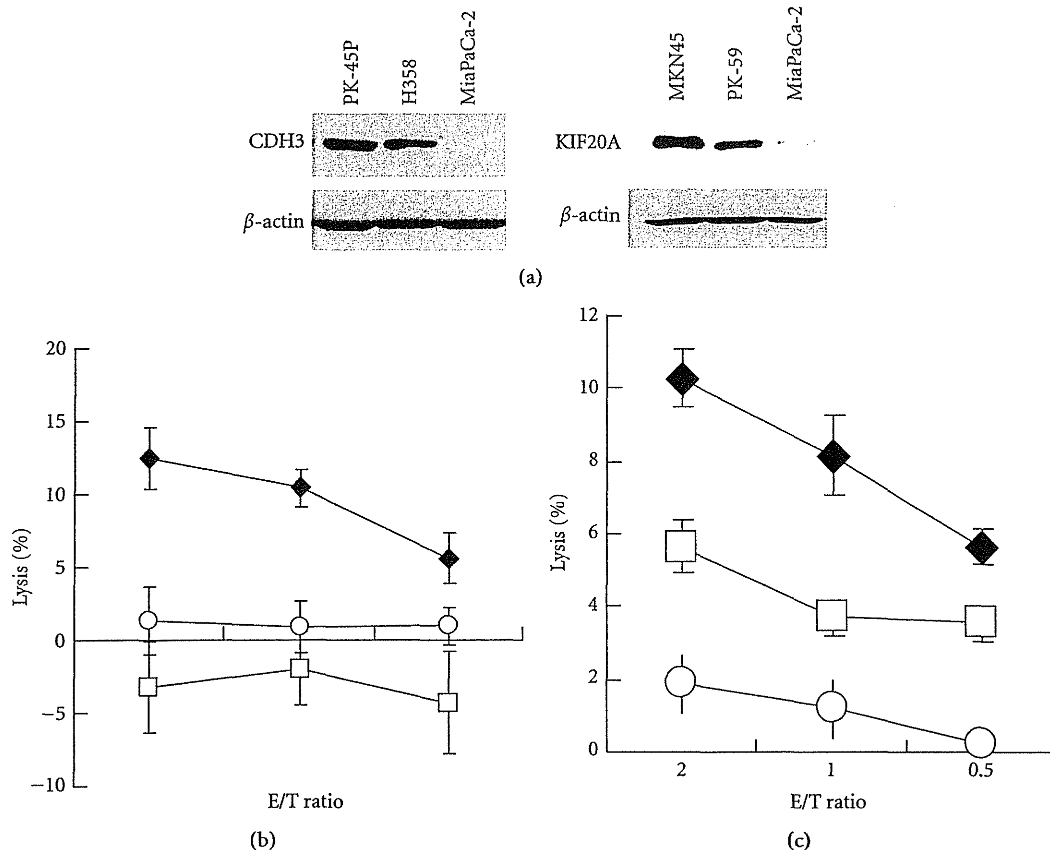

FIGURE 6: Cytotoxic activity against tumor cells expressing respective gene. (a) The expression of CDH3 and KIF20A protein in tumor cells used in cytotoxic assay. (b) Cytotoxic activity of CDH3-10-807 peptide-specific CTL clone against CDH3-expressing HLA-A*2402-positive PK-45P cells (closed diamond), CDH3-expressing HLA-A*2402-negative H358 cells (open square), or MiaPaCa-2 cells (open circle). Cytotoxicity against PK-45P cells was significantly higher than those against other cells. (c) Cytotoxic activity of KIF20A-10-66 peptide-specific CTL clone against KIF20A-expressing HLA-A*2402-positive MKN-45 cells (closed diamond), KIF20A-expressing HLA-A*2402-negative PK-59 cells (open square), or MiaPaCa-2 cells (open circle). Cytotoxicity against MKN-45 cells or PK-59 cells are significantly higher than that against MiaPaCa-2 cells, although cytotoxic activity against PK-59 cells was significantly lower compared with that against MKN-45 cells. E/T ratio, effector cell (CTL clone)/target cell (tumor cell) ratio. Similar results were obtained in three independent experiments using same CTL clone and in independent experiments using other CTL clones.

Expression of KIF20A protein was confirmed in HLA-A*2402-positive MKN-45 cells and HLA-A*2402-negative PK-59 cells, but HLA-A*2402-positive MiaPaca-2 cells did not express KIF20A (Figure 6(a)). KIF20A-10-66 peptide-specific CTL clone exerted significant cytotoxic activity against KIF20A-expressing HLA-A*2402-positive MKN-45 cells, but not MiaPaca-2 cells (Figure 6(c)). KIF20A-10-66 peptide-specific CTL clone demonstrated cytotoxic activity against KIF20A-expressing HLA-A*2402-negative PK-59 cells; however, this cytotoxicity was always less when compared with that against KIF20A-expressing HLA-A*2402-positive MKN-45 cells (Figure 6(c) and data not shown).

No homologous sequence to CDH3-10-807 peptide or KIF20A-10-66 peptide was demonstrated by the homology research using the BLAST algorithm http://blast.ncbi.nlm.nih.gov/Blast.cgi (data not shown), suggesting that these peptide would be the unique epitope peptide presented on HLA-A*2402 of CDH3 or KIF20A-expressing cells.

Taken together, presented results suggested that CDH3-10-807 peptide-specific or KIF20A-10-66 peptide-specific CTLs exert potent IFN-γ production and cytotoxic activity specifically responding to HLA-A*2402-positive cancer cells expressing CDH3 or KIF20A, respectively.

4. Discussion

Pancreatic cancer is one of the most malignant cancers, since 5-year survival rate is only 5% and the therapeutic modalities are very limited [26, 27]. Both CDH3 and KIF20A were upregulated in the majority of pancreatic cancers and have oncogenic functions [15, 16]. Thus, CDH3 and KIF20A would be promising target molecules to develop novel therapeutic strategies for pancreatic cancer. Hence, we identified HLA-A*0201-restricted peptides derived from CDH3 and KIF20A [28, 29].

In present study, we successfully identified HLA-A*2402-restricted novel epitope peptides derived from both CDH3 and KIF20A and demonstrated that these peptides could induce specific CTLs producing potent amount of IFN-γ and

exert cytotoxic activity. Established CDH3-10-807-specific CTL clones or KIF20A-10-66-specific CTL clones responded to CDH3- or KIF20A-introduced COS7 cells as well as CDH3 or KIF20A endogenously expressing cancer cells (PK-45P or MKN-45) in HLA-A24-restricted manner. These results indicated that induction of CDH3-10-807-specific CTLs or KIF20A-10-66-specific CTLs would exert antitumor effect against pancreatic cancers in HLA-A24-positive patients.

Predicted binding score of KIF20A-10-66 peptide to HLA-A*2402 was relatively low when compared with that of CDH3-10-807 peptide. We previously reported epitope peptides derived from RNF43 and IMP-3, and those peptides also have low affinity to HLA molecule [22, 24]. Interestingly, both peptides have been already applied for clinical trials as peptide-based immunotherapy and CTL were obtained in many cancer patients [11, 12]. These results suggested that some peptides possibly induce CTLs albeit binding score was low by BIMAS prediction and KIF20A-10-66 peptide, as well as CDH3-10-807 peptide, possibly induces CTL in cancer patients.

Recent improvement and development of cancer therapies, including combined treatments of standard therapies (chemotherapy, radiotherapy, and surgical resection), substantially improved the survival of advanced cancer patients [27]. However, unfavorable adverse events are still often observed. On the other hand, immune therapies inducing cancer-cell-specific CTLs are now developed to improve the efficacy against cancers and the quality of life of patients. Ongoing several clinical trials using epitope peptides derived from TAA have been proving the evidence that CTL-inducing therapies are much less harmful to the patients [10–12]. However, efficacy of some vaccine therapy trials is still limited mainly due to the development of escaping variant cancer cells that lost targeted TAA expression during the treatment [30]. Therefore, it is generally thought that the therapeutic efficacy would be improved when the origin of vaccinated peptide is functionary essential molecule for cancer cell survival, proliferation, and/or motility. We have been screening epitope peptides derived from cancer-specific genes and reported several epitope peptides, which can elicit specific CTL responses [21–24]. Some of these peptides have been already applied for translational researches of multipeptide vaccine to treat esophageal cancer and colorectal cancer [11, 12]. Moreover, multiple-antigen vaccine therapy was suggested to more effectively hinder escape mechanisms in the guidance from Food and Drug Administration (Guidance for Industry: Clinical Considerations for Therapeutic Cancer Vaccines). Thus, we believe that identification of CTL-inducible epitope peptides derived from several molecules that play critical roles in various types of cancer is important to develop multipeptide cocktail, and that resulted in the improvement of efficacy of CTL-inducing cancer therapies.

Presented results demonstrated that CDH3-10-807 peptide and KIF20A-10-66 peptide pulsed DCs induced specific CTL to possibly exert antitumor effect. The immunogenicity of CDH3-10-807 peptide and KIF20A-10-66 peptide should be examined in patients bearing these genes-expressing cancers, and we are now going to conduct clinical trials.

References

[1] T. Boon, "Tumor antigens recognized by cytolytic T lymphocytes: present perspectives for specific immunotherapy," *International Journal of Cancer*, vol. 54, no. 2, pp. 177–180, 1993.

[2] T. Boon and P. Van der Bruggen, "Human tumor antigens recognized by T lymphocytes," *Journal of Experimental Medicine*, vol. 183, no. 3, pp. 725–729, 1996.

[3] P. van der Bruggen, C. Traversari, P. Chomez et al., "A gene encoding an antigen recognized by cytolytic T lymphocytes on a human melanoma," *Science*, vol. 254, no. 5038, pp. 1643–1647, 1991.

[4] V. Brichard, A. Van Pel, T. Wolfel et al., "The tyrosinase gene codes for an antigen recognized by autologous cytolytic T lymphocytes on HLA-A2 melanomas," *Journal of Experimental Medicine*, vol. 178, no. 2, pp. 489–495, 1993.

[5] Y. Kawakami, S. Eliyahu, K. Sakaguchi et al., "Identification of the immunodominant peptides of the MART-1 human melanoma antigen recognized by the majority of HLA-A2-restricted tumor infiltrating lymphocytes," *Journal of Experimental Medicine*, vol. 180, no. 1, pp. 347–352, 1994.

[6] Y. T. Chen, M. J. Scanlan, U. Sahin et al., "A testicular antigen aberrantly expressed in human cancers detected by autologous antibody screening," *Proceedings of the National Academy of Sciences of the United States of America*, vol. 94, no. 5, pp. 1914–1918, 1997.

[7] S. R. Reynolds, A. Zeleniuch-Jacquotte, R. L. Shapiro et al., "Vaccine-induced $CD8^+$ T-cell responses to MAGE-3 correlate with clinical outcome in patients with melanoma," *Clinical Cancer Research*, vol. 9, no. 2, pp. 657–662, 2003.

[8] S. A. Rosenberg, J. C. Yang, D. J. Schwartzentruber et al., "Recombinant fowlpox viruses encoding the anchor-modified gp100 melanoma antigen can generate antitumor immune responses in patients with metastatic melanoma," *Clinical Cancer Research*, vol. 9, no. 8, pp. 2973–2980, 2003.

[9] G. Pecher, A. Häring, L. Kaiser, and E. Thiel, "Mucin gene (MUC1) transfected dendritic cells as vaccine: results of a phase I/II clinical trial," *Cancer Immunology, Immunotherapy*, vol. 51, no. 11-12, pp. 669–673, 2002.

[10] M. Miyazawa, R. Ohsawa, T. Tsunoda et al., "Phase I clinical trial using peptide vaccine for human vascular endothelial growth factor receptor 2 in combination with gemcitabine for patients with advanced pancreatic cancer," *Cancer Science*, vol. 101, no. 2, pp. 433–439, 2010.

[11] K. Kono, Y. Mizukami, Y. Daigo et al., "Vaccination with multiple peptides derived from novel cancer-testis antigens can induce specific T-cell responses and clinical responses in advanced esophageal cancer," *Cancer Science*, vol. 100, no. 8, pp. 1502–1509, 2009.

[12] K. Okuno, F. Sugiura, J. I. Hida et al., "Phase I clinical trial of a novel peptide vaccine in combination with UFT/LV for metastatic colorectal cancer," *Experimental and Therapeutic Medicine*, vol. 2, no. 1, pp. 73–79, 2011.

[13] M. Palmer, J. Parker, S. Modi et al., "Phase I study of the BLP25 (MUC1 peptide) liposomal vaccine for active specific immunotherapy in stage IIIB/IV non-small-cell lung cancer," *Clinical Lung Cancer*, vol. 3, no. 1, pp. 49–57, 2001.

[14] T. Nakamura, Y. Furukawa, H. Nakagawa et al., "Genome-wide cDNA microarray analysis of gene expression profiles in pancreatic cancers using populations of tumor cells and normal ductal epithelial cells selected for purity by laser microdissection," *Oncogene*, vol. 23, no. 13, pp. 2385–2400, 2004.

[15] K. Taniuchi, H. Nakagawa, M. Hosokawa et al., "Overexpressed P-cadherin/CDH3 promotes motility of pancreatic cancer cells by interacting with p120ctn and activating Rho-family GTPases," *Cancer Research*, vol. 65, no. 8, pp. 3092–3099, 2005.

[16] K. Taniuchi, H. Nakagawa, T. Nakamura et al., "Down-regulation of RAB6KIFL/KIF20A, a kinesin involved with membrane trafficking of discs large homologue 5, can attenuate growth of pancreatic cancer cell," *Cancer Research*, vol. 65, no. 1, pp. 105–112, 2005.

[17] M. Takeichi, "The cadherins: cell-cell adhesion molecules controlling animal morphogenesis," *Development*, vol. 102, no. 4, pp. 639–655, 1988.

[18] F. Lai, A. A. Fernald, N. Zhao, and M. M. Le Beau, "cDNA cloning, expression pattern, genomic structure and chromosomal location of RAB6KIFL, a human kinesin-like gene," *Gene*, vol. 248, no. 1-2, pp. 117–125, 2000.

[19] Y. Ikeda-Moore, H. Tomiyama, K. Miwa et al., "Identification and characterization of multiple HLA-A24-restricted HIV-1 CTL epitopes: strong epitopes are derived from V regions of HIV-1," *Journal of Immunology*, vol. 159, no. 12, pp. 6242–6252, 1997.

[20] E. Celis, V. Tsai, C. Crimi et al., "Induction of anti-tumor cytotoxic T lymphocytes in normal humans using primary cultures and synthetic peptide epitopes," *Proceedings of the National Academy of Sciences of the United States of America*, vol. 91, no. 6, pp. 2105–2109, 1994.

[21] H. Ishizaki, T. Tsunoda, S. Wada, M. Yamauchi, M. Shibuya, and H. Tahara, "Inhibition of tumor growth with antiangiogenic cancer vaccine using epitope peptides derived from human vascular endothelial growth factor receptor 1," *Clinical Cancer Research*, vol. 12, no. 19, pp. 5841–5849, 2006.

[22] N. Uchida, T. Tsunoda, S. Wada, Y. Furukawa, Y. Nakamura, and H. Tahara, "Ring finger protein 43 as a new target for cancer immunotherapy," *Clinical Cancer Research*, vol. 10, no. 24, pp. 8577–8586, 2004.

[23] S. Wada, T. Tsunoda, T. Baba et al., "Rationale for antiangiogenic cancer therapy with vaccination using epitope peptides derived from human vascular endothelial growth factor receptor 2," *Cancer Research*, vol. 65, no. 11, pp. 4939–4946, 2005.

[24] T. Suda, T. Tsunoda, Y. Daigo, Y. Nakamura, and H. Tahara, "Identification of human leukocyte antigen-A24-restricted epitope peptides derived from gene products upregulated in lung and esophageal cancers as novel targets for immunotherapy," *Cancer Science*, vol. 98, no. 11, pp. 1803–1808, 2007.

[25] K. Takeda, N. Yamaguchi, H. Akiba et al., "Induction of tumor-specific T cell immunity by anti-DR5 antibody therapy," *Journal of Experimental Medicine*, vol. 199, no. 4, pp. 437–448, 2004.

[26] A. Sultana, C. Tudur Smith, D. Cunningham et al., "Systematic review, including meta-analyses, on the management of locally advanced pancreatic cancer using radiation/combined modality therapy," *British Journal of Cancer*, vol. 96, no. 8, pp. 1183–1190, 2007.

[27] A. Jemal, R. Siegel, E. Ward, Y. Hao, J. Xu, and M. J. Thun, "Cancer statistics, 2009," *CA Cancer Journal for Clinicians*, vol. 59, no. 4, pp. 225–249, 2009.

[28] K. Imai, S. Hirata, A. Irie et al., "Identification of a novel tumor-associated antigen, cadherin 3/P-cadherin, as a possible target for immunotherapy of pancreatic, gastric, and colorectal cancers," *Clinical Cancer Research*, vol. 14, no. 20, pp. 6487–6495, 2008.

[29] K. Imai, S. Hirata, A. Irie et al., "Identification of HLA-A2-restricted CTL epitopes of a novel tumour-associated antigen, KIF20A, overexpressed in pancreatic cancer," *British Journal of Cancer*, vol. 104, no. 2, pp. 300–307, 2011.

[30] J. H. Sampson, A. B. Heimberger, G. E. Archer et al., "Immunologic escape after prolonged progression-free survival with epidermal growth factor receptor variant III peptide vaccination in patients with newly diagnosed glioblastoma," *Journal of Clinical Oncology*, vol. 28, no. 31, pp. 4722–4729, 2010.

Original Paper

Digestive Surgery

Dig Surg 2012;29:132–139
DOI: 10.1159/000337306

Received: October 19, 2011
Accepted after revision: February 13, 2012
Published online: April 24, 2012

Identification of the Lymphatic Drainage Pathways from the Pancreatic Head Guided by Indocyanine Green Fluorescence Imaging during Pancreaticoduodenectomy

Seiko Hirono Masaji Tani Manabu Kawai Ken-ichi Okada Motoki Miyazawa Atsushi Shimizu Kazuhisa Uchiyama Hiroki Yamaue

Second Department of Surgery, Wakayama Medical University School of Medicine, Wakayama, Japan

Key Words
Lymphatic drainage pathway · Pancreatic head · Indocyanine green fluorescence imaging · Optimal lymphadectomy for pancreatic cancer

Abstract
Aims: We identified the lymphatic drainage pathways from the pancreatic head guided by indocyanine green (ICG) fluorescence imaging to analyze optimal lymphadectomy for pancreatic cancer. ***Methods:*** The lymphatic pathways in 20 patients undergoing pancreaticoduodenectomy were analyzed. We injected ICG into the parenchyma in the anterior (n = 10) or posterior surface (n = 10) of the pancreas head and observed the intraoperative lymphatic flows by ICG fluorescence imaging. ***Results:*** The seven main lymphatic drainage pathways were identified: (1) along the anterior or posterior pancreaticoduodenal arcade, (2) running obliquely down behind the superior mesenteric vein (SMV), (3) reaching the left side of the superior mesenteric artery (SMA), (4) running longitudinally upward between the SMV and SMA, (5) along the middle colic artery toward the transverse colon, (6) reaching the paraaortic (PA) region, and (7) reaching the hepatoduodenal ligament. The lymphatic pathway reaching the left side of the SMA was observed in 4 patients (20%), while that reaching the PA region in 17 patients (85%). The mean time to reach around the SMA was longer than that to reach the PA region. ***Conclusions:*** We found that several lymphatic drainage routes were observed from the pancreatic head, suggesting that a lymphadectomy around the SMA might have a similar oncological impact as that of the PA region.
Copyright © 2012 S. Karger AG, Basel

Introduction

Pancreatic cancer generally has a poor prognosis because the incidence of invasion of extrapancreatic fatty tissue, including lymphatic vessels and nerves, and distant metastasis is high [1–3]. The only chance of cure for pancreatic cancer is surgical resection followed by adjuvant chemotherapy [4]; however, the 5-year survival rate of patients undergoing curative resection remains a mere 7–25% [1–3]. Especially lymph node metastasis is the most important prognostic factor in the patients after surgical resection of pancreatic cancer [5–8]. Therefore, many surgeons have tried to perform an extended lymphadectomy as one strategy for improving survival in the patients with pancreatic cancer [9–12], since Fort-

KARGER
Fax +41 61 306 12 34
E-Mail karger@karger.ch
www.karger.com

© 2012 S. Karger AG, Basel
0253–4886/12/0292–0132$38.00/0

Accessible online at:
www.karger.com/dsu

Hiroki Yamaue, MD
Second Department of Surgery
Wakayama Medical University School of Medicine
811-1 Kimiidera, Wakayama 641-8510 (Japan)
Tel. +81 73 441 0613, E-Mail yamaue-h@wakayama-med.ac.jp

ner [13] initially proposed 'regional pancreatectomy as en-bloc resection for pancreatic cancer with the lymphatic vessels and great vessels' in 1973. However, four prospective, randomized controlled studies were performed to analyze the potential advantage or disadvantage of an extended lymphadectomy in the patients with pancreatic head cancer, and it was suggested that the extended procedure did not benefit the overall survival, and there might even be a trend towards increased morbidity, including diarrhea and delayed gastric emptying [14–17].

Several reports have emphasized the importance of lymphadectomy along the superior mesenteric artery (SMA), including the first, second, and third jejunal arteries (J1, J2, and J3 regions) for locoregional control and improvement of survival in the patients with pancreatic head cancer [18–21]. They reported that the tissue adherent to the SMA might cause local recurrence after surgery, because the tissue contained the lymphatic structures from the uncinate process of the pancreas [22, 23], therefore they concluded that the circumferential clearance of the SMA, including J1, J2, and J3 regions, was needed in pancreatic head cancer [18, 19]. In all studies comparing the standard pancreatoduodenectomy (PD) and PD with extended lymphadectomy, extended lymphadectomy was focused on paraaortic (PA) lymph node dissection, but not lymph node dissection around the SMA, therefore no evidence was observed regarding the significance of the circumferential clearance of the SMA in pancreatic cancer.

Recently, an instrument providing fluorescence imaging of lymphatic flow, the photodynamic eye (PDE; Hamamatsu Photonics, Hamamatsu, Japan) [24], has been used in experimental and preliminary clinical studies for breast cancer and gastrointestinal cancer [25–28]. The indocyanine green (ICG) reagent is a 776-Da disulfonated small molecule and ICG absorbs light in the near-infrared range, with the maximum at a wavelength of 800 nm, and also emits maximal fluorescence at a wavelength of 840 nm when it binds to plasma proteins [29–32]. ICG fluorescence imaging has been reported to make it easy to distinguish lymphatic vessels and lymph nodes containing ICG particles from the surrounding tissue [24–28]. The PDE system, guided by ICG, can visualize the lymphatic drainage flow in the operating room in a real-time fashion [24–28].

The purpose of our study was to verify that extended lymphadectomy does not provide any substantial benefit regarding the locoregional control of pancreatic cancer, by visualizing the lymphatic pathway from the pancreatic head, using ICG fluorescence imaging. We first tried to identify the lymphatic pathways from the pancreatic head, by this new method using the PDE system, to analyze optimal lymphadectomy including that around the SMA basis on the lymphatic flows.

Materials and Methods

Patients

Our series consisted of 20 consecutive patients prospectively recruited who met the eligibility criteria of undergoing conventional pancreaticoduodenectomy (PD), pylorus-preserving PD (PpPD) or pylorus-resecting PD (PrPD) between October 2008 and June 2009 at Wakayama Medical University Hospital (WMUH).

The eligibility criteria were: (1) the maximum tumor diameter was <3 cm and located in the head of the pancreas, because massive cancerous invasion or intense desmoplastic reaction causes obstruction of the lymphatic vessels, and the dye would then be unable to follow the normal lymphatic flow, and (2) the age of the patients was <80 years. None of the patients received either chemotherapy or irradiation preoperatively. The procedures for this study were approved by the ethics committee of WMUH (No. 600), and written informed consent was obtained from each of the patients before he/she was included in this study.

Optimal Dose of ICG

To determine the optimal dose of ICG, we did the following: 25 mg of ICG (Diagnogreen; Daiichi Pharmaceutical, Tokyo, Japan) was diluted in a total of 5 ml. At first, the ability to observe lymphatic drainage was examined at 0.1 ml in 4 patients, but it was difficult to find the lymphatic flows with PDE in 2 of these patients (50%). Next, we checked the lymphatic drainage using 0.2 ml, and found that we could clearly observe the lymphatic flows that received ICG with PDF in all 4 patients (100%). Finally the ability to observe lymphatic drainage was examined at 0.4 ml. However, at this level, we could not distinguish lymphatic vessels from the surrounding adipose tissue, because ICG spread diffusely and was visualized as large shining fluorescent spots with PDE in 3 of the 4 patients (75%). On the basis of these results, we decided to inject 0.2 ml throughout the subsequent experiments using the 20 enrolled patients. Injection into the parenchyma in the anterior or posterior surface was alternately selected in the enrolled patients.

Technique

After laparotomy, Kocher's maneuver was performed carefully, and then gastric or duodenal resection was performed. A 0.2-ml aliquot of 0.5% ICG solution was injected into the parenchyma in the anterior or posterior surface of the uncinate process of the pancreas with a 26-gauge needle at a depth of 0.5 mm.

We observed intraoperative lymphatic drainage flows from the uncinate process of the pancreas by ICG fluorescence imaging using the PDE system. The fluorescence signals were transmitted to a digital video processor to be displayed on a TV monitor in real time. We assessed the pattern of spread of the ICG by the PDE for the initial 15 min after ICG injection, and also observed the

Table 1. Clinicopathological characteristics of the patients injected with ICG

No.	Age	Sex	Final histopathological diagnosis	Tumor size, cm	Operation	TNM stage[1]	Perineural invasion	Ratio of N+/N−
Patients injected with ICG into the anterior surface of the uncinate pancreas								
1	62	M	distal bile duct cancer	2.5	PrPD	T3, N1, M0; stage IIB	positive	2/11
2	77	F	distal bile duct cancer	1.2	PpPD	T3, N1, M0; stage IIB	positive	7/17
3	63	M	distal bile duct cancer	1.4	PrPD	T3, N0, M0; stage IIA	negative	0/13
4	69	M	pancreatic ductal adenocarcinoma	2.9	PrPD	T3, N1, M0; stage IIB	negative	2/13
5	70	F	pancreatic ductal adenocarcinoma	2.2	PrPD + SMV resection	T3, N1, M0; stage IIB	negative	1/33
6	61	F	pancreatic ductal adenocarcinoma	1.0	PrPD	T1, N0, M0; stage IA	negative	0/10
7	72	M	pancreatic ductal adenocarcinoma	2.8	PrPD + SMV resection	T3, N1, M0; stage IIB	negative	2/22
8	75	M	distal bile duct cancer	1.5	PpPD	T1, N1, M0; stage IIB	negative	4/21
9	58	F	chronic pancreatitis (tumor forming)	2.0	PrPD	–	–	–
10	67	F	pancreatic ductal adenocarcinoma	2.0	PD	T3, N0, M0; stage IIA	negative	0/11
Patients injected with ICG into the posterior surface of the uncinate pancreas								
11	69	F	pancreatic ductal adenocarcinoma	1.5	PpPD	T1, N0, M0; stage IA	negative	0/36
12	68	M	pancreatic ductal adenocarcinoma	2.3	PrPD	T3, N1, M0; stage IIB	negative	3/11
13	60	M	pancreatic ductal adenocarcinoma	1.8	PrPD	T3, N0, M0; stage IIA	negative	1/19
14	75	M	distal bile duct cancer	1.4	PrPD	T3, N1, M0; stage IIB	positive	1/29
15	65	F	pancreatic ductal adenocarcinoma	1.5	PpPD	T3, N0, M0; stage IIA	negative	0/14
16	75	F	pancreatic ductal adenocarcinoma	2.3	PrPD + SMV resection	T3, N1, M0; stage IIB	negative	2/27
17	71	M	pancreatic ductal adenocarcinoma	1.6	PrPD	T1, N1, M0; stage IIB	negative	2/15
18	79	F	distal bile duct cancer	1.3	PrPD	T3, N0, M0; stage IIA	negative	0/12
19	64	F	pancreatic ductal adenocarcinoma	1.0	PrPD	T1, N0, M0; stage IA	negative	0/12
20	53	M	pancreatic ductal adenocarcinoma	2.5	PrPD + SMV resection	T3, N1, M0; stage IIB	negative	4/45

[1] TNM classification of the Union internationale contre le cancer.

lymphatic flow at the time of resection of the bile duct (mean 50 min, range 29–110) and resection of the pancreas (mean 87 min, range 57–137). We performed sampling or dissection en bloc of tissue received ICG and then diagnosed these tissues in pathological examination.

Results

Patient Characteristics

Table 1 shows the clinicopathological characteristics of the patients in this study. The patients included 10 males and 10 females, with an average age of 68.2 ± 6.7 years (range 53–79). The final pathological diagnosis showed that 13 patients had pancreatic ductal adenocarcinoma, 6 had distal bile duct cancer, and 1 had tumor-forming pancreatitis. The mean size of the pancreatic tumors was 1.9 ± 0.6 cm (range 1.0–2.9). According to the UICC TNM classification [33], among 13 patients with pancreatic ductal carcinoma, 3 patients were stage IA, 3 patients were IIA, and 7 patients were stage IIB, while among the 6 patients with bile duct cancer, 2 patients were stage IIA and 4 patients were stage IIB. According to pathological examinations, 3 patients (15.8%) had perineural invasion and 10 patients (52.6%) had lymph node metastasis. 15 patients underwent PrPD, 4 PpPD, and 1 PD, and 4 patients also underwent a combined the superior mesenteric vein (SMV) resection.

Lymphatic Pathways from the Uncinate Process of the Pancreas and the Mean Time to Arrive at the Drainage Areas

There were no patients with complications or adverse events related to intraoperative injection of ICG, regardless of the dose (up to 0.4 ml). Immediately after the ICG injection, we were able to locate the lymphatic vessels draining the uncinate process of the pancreas as shining fluorescent streams and spots in fluorescence images of the PDE, whereas no lymphatic flow was clearly visible as green in color after ICG injection, and could not be easily judged as being lymphatic vessels by naked-eye examination.

The lymphatic drainage routes from the uncinate process of the pancreas detected with PDE are shown in tables 2 and 3. Seven main lymphatic pathways from the

Table 2. Lymphatic drainage pathways in the patients injected with ICG into the anterior surface of the uncinate process of the pancreas

No.	Anterior pancreaticoduodenal arcade	Behind the SMV	Left side of the SMA (J1, J2, J3 regions)	Longitudinally upward between the SMV and SMA	Origin of the middle colonic artery toward the transverse colon	PA region	Hepatoduodenal ligament
1	○	○	○	○	○	○	×
2	○	○	○	○	○	○	×
3	○	○	○	×	○	○	×
4	○	○	×	○	○	○	×
5	○	○	○	×	○	○	×
6	○	○	×	×	○	○	×
7	○	○	×	×	○	○	×
8	○	○	×	○	○	×	×
9	○	○	×	×	×	○	×
10	○	○	×	×	○	×	×

Table 3. Lymphatic drainage pathways in the patients injected with ICG into the posterior surface of the uncinate process of the pancreas

No.	Posterior pancreaticoduodenal arcade	Behind the SMV	Left side of the SMA (J1, J2, J3 regions)	Longitudinally upward between the SMV and SMA	Origin of the middle colonic artery toward the transverse colon	PA region	Hepatoduodenal ligament
11	○	○	×	○	○	○	×
12	○	○	×	×	○	○	×
13	○	○	×	○	×	○	○
14	○	○	×	○	○	○	×
15	○	○	×	○	×	○	○
16	○	○	×	○	×	○	×
17	○	○	×	×	×	○	○
18	○	×	×	×	×	○	×
19	○	×	×	×	×	○	×
20	○	×	×	×	×	×	×

uncinate process of the pancreas were observed with PDE. The lymphatic pathways were observed (1) along the anterior or posterior pancreaticoduodenal arcade, (2) running obliquely down behind the SMV, (3) passing behind the SMV and SMA and reaching the left side of the SMA (J1, J2, or J3 regions), (4) passing behind the SMV and running longitudinally upward between the SMV and SMA, (5) passing the origin of the middle colonic artery toward the transverse colon, (6) reaching the PA region, and (7) reaching the hepatoduodenal ligament.

Table 2 shows the lymphatic drainage pathways in the patients with injection of ICG into the anterior surface of the uncinate process of the pancreas (n = 10). We could identify the lymphatic flow along the anterior pancreaticoduodenal arcade in all 10 patients (100%) within 5 min after ICG injection. The lymphatic flow running obliquely down and shining fluorescent spots behind the SMV were found in all 10 patients (100%) with an ICG injection into the anterior surface, and then the lymphatic flow reaching on the left side of the SMA (J1, J2, or J3 region) was observed in 4 patients (40%). We observed the lymphatic flow running longitudinally upward between the SMV and SMA from the anterior surface in 4 patients (40%). Shining at the origin of the middle colonic artery was observed in 9 patients (90%) with the anterior injection. The lymphatic flow reaching the PA region was found in 8 patients (80%) who receive an ICG injection into the anterior surface, whereas the lymphatic flow reaching the hepatoduodenal ligament was not found in any patients with the anterior injection.

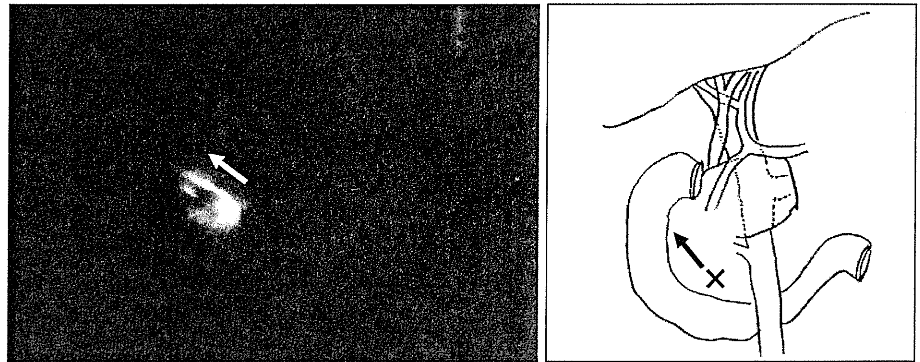

Fig. 1. Lymphatic flow from the anterior surface of the uncinate process of the pancreas toward the duodenal wall and then spread along the anterior pancreaticoduodenal arcade. × = Injection site, the arrow indicates the lymphatic flow visualized by the ICG fluorescence imaging system.

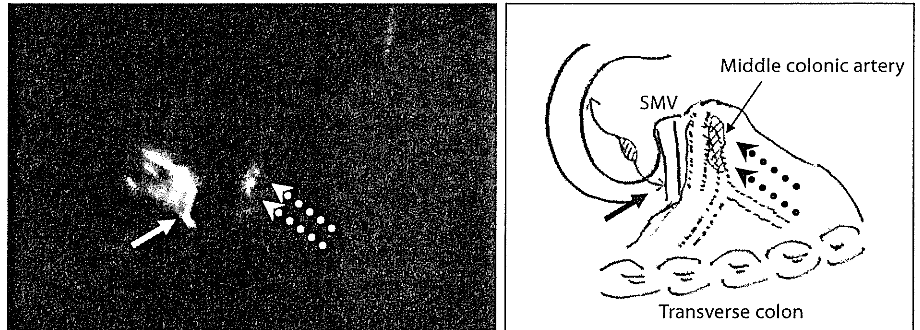

Fig. 2. Lymphatic flow running obliquely down behind the SMV was observed (a solid arrow), and at the same time, a shining spot at the origin of the middle colonic artery was observed (dotted arrows) in the patient who received an anterior injection.

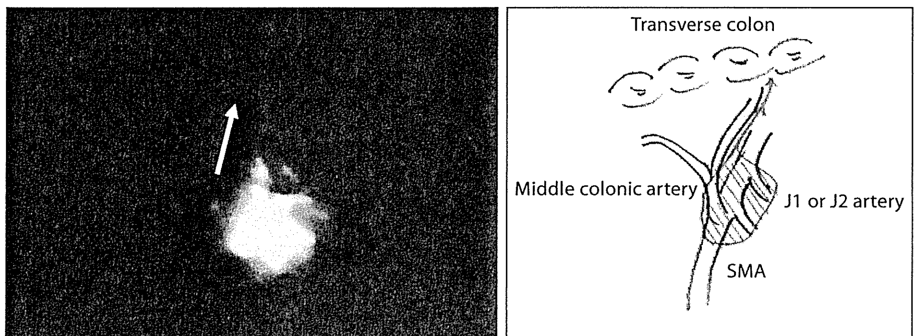

Fig. 3. Shining spots on the left side area of the SMA (J1 or J2) were observed in the patient who received an anterior injection. The lymphatic flow moving to the transverse colon through the middle colonic artery was observed.

Table 3 shows the lymphatic drainage pathways in the patients with an ICG injection into the posterior surface of the uncinate process (n = 10). We observed the lymphatic flow along the posterior pancreaticoduodenal arcade in all 10 patients (100%) immediately after ICG injection into the posterior surface. The lymphatic flow running obliquely down behind the SMV from the posterior surface of the uncinate process was found in 7 patients (70%), but reaching on the left side of the SMA was not observed in any patients with an ICG injection into the posterior surface. The lymphatic flow running longitudinally upward between the SMV and SMA from the posterior surface was observed in 5 patients (50%), and the lymphatic flow passing the origin of the middle colonic artery toward the transverse colon was observed in 3 patients (30%) with the posterior injection. The lymphatic flow reaching the PA region was found in 9 patients (90%) who received an ICG injection into the posterior surface, and the lymphatic flows reaching the hepatoduodenal ligament in 3 patients (30%).

Figure 1 shows the lymphatic flow toward the duodenal wall and then along the anterior pancreaticoduodenal arcade in case 1, with the injection of ICG at the anterior surface of the pancreas head. Figure 2 shows the lymphatic flow running obliquely down behind the SMV, and at the same time, the shining spot at the origin of the middle colonic artery, when ICG was injected in the anterior surface (case 1). Figure 3 shows the shining spots on the left side of the SMA (J1 and J2 regions), and the lymphatic flow passing the origin of the middle colic ar-

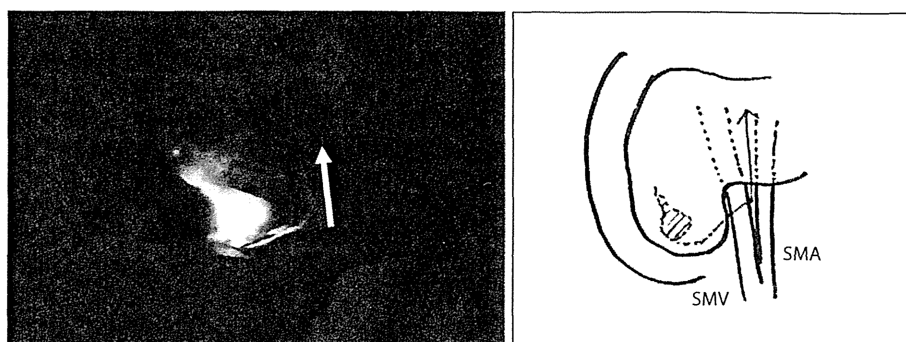

Fig. 4. Lymphatic flow running longitudinally upward between the SMV and SMA was observed in the patient who received a posterior injection.

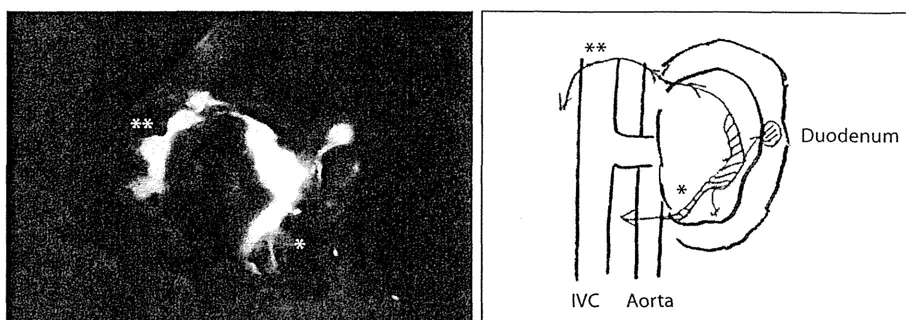

Fig. 5. Shining spots in the PA area were observed. There were two routes toward the PA area; one was the flow directly from the posterior pancreatic head (*), and the other was the flow passing the origin of the SMA toward the anterior inferior vena cava (**).

Table 4. Mean time to arrival at the shining spots from the uncinate process of the pancreas

Injection	Anterior or posterior pancreaticoduodenal arcade	Behind the SMV	Left side of the SMA (J1, J2, J3 regions)	Longitudinally upward between the SMV and SMA	Origin of the middle colonic artery toward the transverse colon	PA region	Hepatoduodenal ligament
Anterior surface of the uncinate process	2.0 min (0.5–4.5)	10.7 min (5–30)	41.8 min (7–80)	21.3 min (10–30)	8.4 min (1–30)	8.2 min (1–30)	–
Posterior surface of the uncinate process	1.6 min (0.5–4)	50.3 min (5–80)	–	38.2 min (5–78)	35.0 min (25–50)	7.2 min (1–50)	38 min (4–60)

Values in parentheses show the range of time to arrive after ICG injection.

tery toward the transverse colon in case 1, with the anterior injection. Figure 4 shows the lymphatic flow running longitudinally upward between the SMV and SMA when ICG was injected into the posterior surface (case 14). Figure 5 shows the lymphatic pathways reaching the PA regions from the anterior surface of the uncinate process (case 1). There were two routes that were observed to shine in the PA area; one was the lymphatic flow directly to the PA area from the posterior surface of the pancreas, and the other was the lymphatic flow passing the origin of the SMA toward the PA area, and then passing the anterior inferior vena cava and reaching the right side of the inferior vena cava.

The mean time to arrive at the each of the shining spots after ICG injection is shown in table 4. The mean arrival time of the drainage pathway reaching around the SMA was longer than that reaching the PA region following both the anterior and posterior injections (21.3 min, 38.2 vs. 8.1 min, 7.2 min).

Histopathological Examination of Tissues That Received ICG

We performed sampling of the PA tissue received in 11 of the 13 patients with pancreatic cancer who were found to have lymphatic flow to the PA tissue. None of the sampled tissue specimens contained malignant deposits on final histopathological examination. In only 1 patient with pancreatic cancer in whom we had observed shining in the left side of the SMA, we dissected en bloc the left side region of the SMA, and no malignant cells around the SMA were found in pathological examination.

Discussion

Several studies have tried to identify the lymphatic pathways in pancreatic cancer patients to determine the optimal lymphadectomy procedure, however the pattern of lymphatic drainage and draining areas remained poorly defined [22–35]. Deki and Sato [22] reported the lymphatic pathways of the pancreas by dissecting the lymphatic vessels using a cadaver. This report described that the lymphatic vessels running obliquely down and passing behind the SMA and SMV and linking with lymph nodes located between these vessels and the posterior layer of the mesentery were observed in the anterior pancreatic head. It has also been reported using autopsy specimens that the lymphatic pathway from the posterior pancreatic head drains toward the right or posterior side of the SMA and finally to the PA lymph nodes [23]. Although these studies did provide useful information, as they used only autopsy specimens, they could not identify the physiological lymphatic flow from the pancreas in a real-time fashion. In another study, sentinel lymph node mapping of pancreatic head cancer was studied by methylene blue dye injection, however the study failed and concluded that it was not possible to identify lymphatic drainage from the pancreatic head using their technology [34].

In this study, we injected ICG into the anterior or posterior surface of the uncinate process of the pancreas, after determining the optimal concentration of ICG by examining various concentrations [28], and then evaluated the time to arrive at the lymphatic drainage areas. The reasons that we chose the uncinate process as injected location of ICG are (1) cancer in the ventral pancreatic head occurs more often than that in the dorsal pancreatic head [20], and (2) it has been reported that lymph node metastasis around the SMA is most often in the cancer located in the uncinate process [18, 19].

We could identify the visual lymphatic drainage pathways from the head of the pancreas by ICG fluorescence imaging during surgery. Indeed, we found the lymphatic root passing behind the SMV and SMA around the left side of the SMA from the anterior pancreatic head, as the previous anatomic reports description, however we also simultaneously found several other roots including the PA region. With regard to the relationship between lymphatic drainage and the clinical significance of lymph node metastasis, of the 16 patients demonstrating lymphatic drainage to the PA region, 6 patients had no lymph node metastasis and 10 patients had lymph node metastasis in only the regional lymph node. As a result, we did not find any relationship between lymphatic drainage and the clinical outcome.

This study showed that (1) the lymphatic drainage to the PA region from the pancreatic head was more often than that to the left side of the SMA (J1, J2, and J3 regions), (2) the patients with lymphatic drainage into the left side of the SMA have a simultaneous pathway into the PA region, and (3) the time reaching around the SMA was longer than that reaching the PA region. Based on these results, a lymphadenectomy of the left side of the SMA, including the J1, J2, and J3 regions, might have a similar oncological impact as a lymphadenectomy around the PA region, that is, the circumferential clearance of the SMA may not be of benefit as PA lymph node dissection is for patients with pancreatic cancer, although prospective randomized controlled studies would be needed to prove our conclusion.

References

1 Michalski CW, Kleef J, Wente MN, et al: Systematic review and meta-analysis of standard and extended lymphadenectomy in pancreaticoduodenectomy for pancreatic cancer. Br J Surg 2007;94:265–273.
2 Pawlik TM, Abdalla EK, Barnett CC, et al: Feasibility of a randomized trial of extended lymphadectomy for pancreatic cancer. Arch Surg 2005;140:584–591.
3 Alexakis N, Halloran C, Raraty M, et al: Current standards of surgery for pancreatic cancer. Br J Surg 2004;91:1410–1427.
4 Stocken DD, Büchler MW, Dervenis C, et al: Meta-analysis of randomized adjuvant therapy trials for pancreatic cancer. Br J Cancer 2005;92:1372–1381.
5 Hirono S, Yamaue H, Hoshikawa Y, et al: Molecular markers associated with lymph node metastasis inn pancreatic ductal adenocarcinoma by genome-wide expression profiling. Cancer Sci 2010;101:259–266.

6 Riediger H, Keck T, Wellner U, et al: The lymph node ratio is the strongest prognostic factor after resection of pancreatic cancer. J Gastrointest Surg 2009;13:1337–1344.
7 Zacharias T, Jaeck D, Neuville OA, et al: Impact of lymph node involvement on long-term survival after R0 pancreaticoduodenectomy for ductal adenocarcinoma of the pancreas. J Gastrointest Surg 2007;11:350–356.
8 Nakao A, Harada A, Nonami T, et al: Lymph node metastases in carcinoma of the head of the pancreas region. Br J Surg 1995;82:399–402.
9 Ishikawa O, Ohhigashi H, Sasaki Y, et al: Practical usefulness of lymphatic and connective tissue clearance for the carcinoma of the pancreas head. Ann Surg 1988;208:215–220.
10 Manabe T, Ohshio G, Baba N, et al: Radical pancreatectomy for ductal cell carcinoma of the head of the pancreas. Cancer 1989;64:1132–1137.
11 Nakao A, Takeda S, Inoue S, et al: Indications and techniques of extended resection for pancreatic cancer. World J Surg 2006;30:976–982.
12 Kato K, Yamada S, Sugimoto H, et al: Prognostic factors for survival after extended pancreatectomy for pancreatic head cancer. Influence of resection margin status on survival. Pancreas 2009;38:605–612.
13 Fortner JG: Regional resection and pancreatic carcinoma. Surgery 1973;73:799–800.
14 Pedrazzoli S, DiCarlo V, Dionigi R, et al: Standard versus extended lymphadenectomy associated with pancreatoduodenectomy in the surgical treatment of adenocarcinoma of the head of the pancreas: a multicenter, prospective, randomized study. Lymphadenectomy Study Group. Ann Surg 1998;228:508–517.
15 Yeo CJ, Cameron JL, Lillemoe KD, et al: Pancreaticoduodenectomy with or without distal gastrectomy and extended retroperitoneal lymphadectomy for periampullary adenocarcinoma. Part 2. Randomized controlled trial evaluating survival, morbidity and mortality. Ann Surg 2002;236:355–366.
16 Farnell MB, Pearson RK, Sarr MG, et al: A prospective randomized trial comparing standard pancreatoduodenectomy with extended lymphadectomy in resectable pancreatic head adenocarcinoma. Surgery 2005;138:618–628.
17 Nimura Y, Nagino M, Kato H, et al: Regional versus extended lymph node dissection in radical pancreaticoduodenectomy for pancreatic cancer: a multicenter, randomized controlled trial (abstract). HPB 2004;6(suppl 1):2.
18 Kayahara M, Nagakawa T, Kobayashi H, et al: Lymphatic flow in carcinoma of the head of the pancreas. Cancer 1992;70:2061–2066.
19 Kayahara M, Nagakawa T, Kobayashi K, et al: Analysis of paraaortic lymph node involvement in pancreatic carcinoma: a significant indication for surgery? Cancer 1999;85:583–590.
20 Kitagawa H, Ohta T, Tani T, et al: Carcinoma of the ventral and dorsal pancreas exhibit different patterns of lymphatic spread. Front Biosci 2008;13:2728–2735.
21 Pessaux P, Varma D, Arnaud FP: Pancreaticoduodenectomy: superior mesenteric artery first approach. J Gastrointest Surg: 2006;10:607–611.
22 Deki H, Sato T: An anatomic of the peripancreatic lymphatics. Surg Radiol Anat 1998;10:121–135.
23 Nagai H, Kuroda A, Morioka Y: Lymphatic and local spread of T1 and T2 pancreatic cancer. Ann Surg 1986;204:65–71.
24 Kitai T, Inomoto T, Miwa M, et al: Fluorescence navigation with indocyanine green for detecting sentinel lymph nodes in breast cancer. Breast Cancer 2005;12:211–215.
25 Ogasawara Y, Ikeda H, Takahashi M, et al: Evaluation of breast lymphatic pathways with indocyanine green fluorescence imaging in patients with breast cancer. World J Surg 2008;32:1924–1929.
26 Tajima Y, Yamazaki K, Masuda Y, et al: Sentinel node mapping guided by indocyanine green fluorescence imaging in gastric cancer. Ann Surg 2009;249:58–62.
27 Kusano M, Tajima Y, Yamazaki K, et al: Sentinel node mapping guided by indocyanine green fluorescence imaging: a new method for sentinel node navigation surgery in gastrointestinal cancer. Dig Surg 2008;25:103–108.
28 Noura S, Ohue M, Seki Y, et al: Feasibility of a lateral region sentinel node biopsy of lower rectal cancer guided by indocyanine green using a near-infrared camera system. Ann Surg Oncol 2010;17:144–151.
29 Caesar J, Shaldon S, Chiandussi L, et al: The use of indocyanine green in the measurement of hepatic blood flow and as a test of hepatic function. Clin Sci 1961;21:43–57.
30 Cherrick GR, Stein SW, Leevy CM, et al: Indocyanine green: observations on its physical properties, plasma decay, and hepatic extraction. J Clin Invest 1960;39:592–600.
31 Nimura H, Narimiya N, Mitsumori M, et al: Infrared ray electronic endoscopy combined with indocyanine green injection for detection of sentinel nodes of patients with gastric cancer. Br J Surg 2004;91:575–579.
32 Ishikawa K, Yasuda K, Shiromizu A, et al: Laparoscopic sentinel node navigation achieved by infrared ray electronic endoscopy system in patients with gastric cancer. Surg Endosc 2007;21:1131–1134.
33 Sobin LH, Wittekind C: International Union Against Cancer. TNM Classification of Malignant Tumor, ed 6. New York, Wiley-Liss, 2002.
34 Kocher HM, Sohail M, Benjamin IS, et al: Technical limitations of lymph node mapping in pancreatic cancer. Eur J Surg Oncol 2007;33:887–891.
35 Evans BP, Ochsner A: The gross anatomy of the lymphatics of the human pancreas. Surgery 1954;36:177–191.

The Carcinoembryonic Antigen Level in Pancreatic Juice and Mural Nodule Size Are Predictors of Malignancy for Branch Duct Type Intraductal Papillary Mucinous Neoplasms of the Pancreas

Seiko Hirono, MD, Masaji Tani, MD, Manabu Kawai, MD, Ken-ichi Okada, MD, Motoki Miyazawa, MD, Atsushi Shimizu, MD, Yuji Kitahata, MD, and Hiroki Yamaue, MD

Objective: Identification of predictors of malignancy for branch duct type intraductal papillary mucinous neoplasms (IPMN).

Background: Main duct type IPMN has been recommended for resection. However, the indications for resection of the branch duct type IPMN have been controversial.

Methods: We retrospectively analyzed the clinicopathological factors of 134 patients undergoing resection for branch duct type IPMN, excluding main duct type IPMN, to identify predictors of the malignant behavior of this neoplasm. The cutoff values of tumor size, main pancreatic duct (MPD) size, mural nodule size, and carcinoembryonic antigen (CEA) level in the pancreatic juice obtained during preoperative endoscopic retrograde pancreatography (ERP) were analyzed using receiver–operator characteristic curves.

Results: We found 7 significant predictors for malignancy in the branch duct type IPMN in a univariate analysis; jaundice, tumor occupying the pancreatic head, MPD size >5 mm, mural nodule size >5 mm, serum carbohydrate antigen (CA)19–9 level, positive cytology in the pancreatic juice, and CEA level in the pancreatic juice >30 ng/mL. In a multivariate analysis, a mural nodule size >5 mm and a CEA level in the pancreatic juice >30 ng/mL were independent factors associated with malignancy. The positive predictive value of a mural nodule size >5 mm and a CEA level in the pancreatic juice >30 ng/mL was 100%, and the negative predictive value was 96.3%.

Conclusions: We identified 2 useful predictive factors for malignancy in branch duct type IPMN; a mural nodule size >5 mm and a CEA level in the pancreatic juice obtained by preoperative ERP >30 ng/mL.

(*Ann Surg* 2012;255:517–522)

As a result of improvements of radiological imaging and increased clinician awareness, intraductal papillary mucinous neoplasm (IPMN) of the pancreas has been recognized with increasing frequency because it was formally defined in 1996 by the World Health Organization.[1] It has been established that IPMN has malignant potential and that it first transforms from an adenoma to a borderline neoplasm, then develops into carcinoma, including carcinoma in situ (CIS), and ultimately becomes an invasive carcinoma [invasive IPMC (intraductal papillary mucinous carcinoma)].[1] In general, IPMN has a favorable prognosis, because of its indolent biological behavior; therefore, excellent survival outcomes have been reported after complete resection in the patients with noninvasive IPMN, including adenoma, borderline neoplasm, and CIS.[2–6] However, once IPMN progresses to invasive carcinoma, it becomes aggressive and is associated with a poor prognosis, with the 5-year survival in patients with invasive IPMC reportedly ranging from 22% to 67%.[7–9] Therefore, the timing of resection is important for the successful treatment of IPMN, and it is necessary to establish a treatment protocol and surgical indications for patients with IPMN.

Depending on the morphology of the changes of the ductal system, IPMNs have been classified into the 3 variations—main duct type, branch duct type, and mixed type by radiological imaging. Many recent clinicopathological studies have shown that IPMNs arising in the main pancreatic duct (MPD) are more aggressive than those arising in the branch pancreatic duct (BPD), and the malignancy rate of main duct type IPMN has been reported to be 57% to 92%,[4–6,10] whereas that of branch duct type IPMN has been reported to be 6% to 58%.[10–14] Therefore, although most clinicians agree that surgical resection is required for all main duct type IPMNs, the management of branch duct type IPMNs remains controversial, because branch duct type IPMN generally has a low risk of malignancy.

We previously suggested that measurement of the carcinoembryonic antigen (CEA) level in the pancreatic juice obtained during preoperative endoscopic retrograde pancreatography (ERP) was useful for distinguishing malignant from benign IPMNs,[2,3]; however, our previous studies had 2 problems: (1) a small number of patients analyzed (n = 54), and (2) the subjects in the study were patients with all types of IPMNs, including the main duct type. Therefore, in the present study, we examined 134 patients with IPMNs, other than the main duct type, and reanalyzed the cutoff values for predicting malignancy of the tumor size, MPD size, mural nodule size, and the CEA level in the pancreatic juice, using receiver–operator characteristic (ROC) curves. We retrospectively analyzed the clinical and imaging findings and laboratory data to identify the predictors of malignancy and determined the optimal indications for the patients with branch duct type IPMN.

MATERIALS AND METHODS

Patient Enrollment

From July 1999 to February 2011, 196 consecutive patients with IPMN underwent a pancreatectomy at Wakayama Medical University Hospital. We classified the patients into 2 groups on the basis of their type of IPMN as determined by preoperative imaging studies; main duct type IPMN and branch duct type IPMN. We defined the main duct type IPMN as that found to have diffuse or segmental MPD dilation, but not cyst formation caused by BPD dilation. Next, we defined the branch duct type IPMN as that with cyst formation caused by BPD dilation with or without MPD dilation. In this study, we excluded 23 patients who had IPMN concomitant with common pancreatic cancer. Among the remaining 173 consecutive patients with resected IPMNs, 134 patients were classified as having branch duct type IPMN, and all were enrolled in this study. The study protocol was approved by the Human Ethics Review Committee of Wakayama Medical University Hospital, and a signed consent form was obtained from each subject.

From the Second Department of Surgery, Wakayama Medical University, School of Medicine, Kimiidera, Wakayama, Japan.

Disclosure: The authors declare that they have nothing to disclose.

Reprints: Hiroki Yamaue, MD, Second Department of Surgery, Wakayama Medical, University, School of Medicine, 811–1 Kimiidera, Wakayama 641–8510, Japan. E-mail: yamaue-h@wakayama-med.ac.jp.

Copyright © 2012 by Lippincott Williams & Wilkins

ISSN: 0003-4932/12/25503-0517
DOI: 10.1097/SLA.0b013e3182444231

Copyright © 2012 Lippincott Williams & Wilkins. Unauthorized reproduction of this article is prohibited.

Preoperative Examination and Indications for Surgery

Before surgery, all patients underwent a clinical evaluation, routine laboratory tests including the assessment of tumor markers, abdominal ultrasonography (US), and computed tomography (CT). Magnetic resonance imaging cholangiopancreatography and endoscopic US (EUS) were performed in 131 and 125 patients, respectively. Endoscopic retrograde pancreatography was performed in all patients with branch duct type IPMN, excluding the 4 patients undergoing Billroth II reconstruction after distal gastrectomy. Preoperative pancreatic juice cytology (n = 104) and measurement of CEA levels in pancreatic juice (n = 91) were performed using the samples obtained during preoperative ERP, using the previously reported method.[2,3] Briefly, the pancreatic juice in the MPD was collected by preoperative ERP, and immediately centrifuged, and the precipitate was used for cytological examination, and the CEA levels in the supernatant were measured by means of a CEA immunometric chemiluminescent assay kit (Bayer Medical Co, Tokyo, Japan). The tumor size was measured by CT, and the mural nodule size was determined by EUS in 125 patients who underwent preoperative EUS, and by CT in other 9 patients without performing EUS.

Surgery was performed in the patients with IPMN who met at least one of the following criteria: (1) the presence of symptoms, (2) main duct type IPMN, (3) the presence of mural nodules, (4) an MPD larger than 7 mm in diameter, or gradual dilation of the MPD observed during follow-up, (5) tumor size larger than 30 mm, or a gradual increase in the tumor size during follow-up, (6) class IV or V in cytology of the pancreatic juice, or (7) a CEA level higher than 110 ng/mL in the pancreatic juice, which was the cutoff level identified by analyzing the difference between benign and malignant IPMNs in all patients with all types of IPMN, using ROC curves, as previously reported.[2,3]

All resected specimens were examined pathologically and classified into adenoma, borderline, CIS, and invasive IPMC, according to the classification established by the World Health Organization by 2 independent pathologists (A.Y. and Y.N.). *Invasive IPMC* was defined as that presenting the pathological findings of continuance of an invasive component from CIS, to distinguish it from common pancreatic ductal cancer concomitant with IPMN.

Statistical Analysis

For the purpose of the analyses, we classified IPMN with adenoma and borderline neoplasm as a benign IPMN group, whereas CIS and invasive IPMC were classified as a malignant IPMN group. The cutoff levels for the tumor size, MPD size, mural nodule size, and CEA level in the pancreatic juice were determined to maximize the difference between benign and malignant IPMNs by ROC curves (SPSS, Release 17.0; SPSS Inc, Chicago, IL). The 16 preoperative potential risk factors were assessed by a univariate analysis with the χ^2 and included the patient age, sex, symptoms, jaundice, body weight loss, abdominal pain, back pain, diabetes mellitus, the tumor location, tumor size, MPD size, mural nodule size, serum CEA level, serum carbohydrate antigen (CA) 19–9 level, cytology in the pancreatic juice, and CEA levels in the pancreatic juice (SPSS, Release 17.0). The $P < 0.1$ predictors of malignant IPMN in the univariate analysis were then included in a forward stepwise multiple logistic regression model (SPSS, Release 17.0). Statistical significance was defined as $P < 0.05$.

RESULTS

Patient Characteristics and Histopathological Findings

Table 1 shows the characteristics of the enrolled patients. This study included 74 men and 60 women, with a mean age ± standard deviation of 68.9 ± 9.7 years. The mean tumor size, mean MPD size, and the mean mural nodule size were 30.4 ± 12.3, 6.5 ± 4.2, and 5.5 ± 5.0, respectively. A total pancreatectomy was performed in 3 patients (2.2%); a pancreatoduodenectomy (PD), including a pylorus-preserving PD and a pylorus-resecting PD, was performed in 101 patients (75.4%); a distal pancreatectomy was performed in 14 patients (10.5%); and a central pancreatectomy was performed in 16 patients (11.9%). Combined venous resection (portal vein or superior mesenteric vein) was performed in 10 patients (7.4%), and combined celiac artery resection was performed in 1 patient (0.8%).

In the 134 patients with branch duct type IPMN, there were 56 patients (41.8%) with benign IPMN, including 51 with adenomas and 5 with borderline neoplasms, and there were 41 patients (30.6%) with CIS, and 37 patients (27.6%) with invasive IPMC, including 5 with minimally invasive IPMC (Table 1).

Complications of ERP and Pancreatic Duct Irrigation

The definition of post-ERP acute pancreatitis and the grading of its severity were based on consensus criteria.[15] Seven patients (5.4%) developed pancreatitis in 130 patients who underwent preoperative ERP. Among them, 5 patients (4.8%) developed pancreatitis (moderate in 1 patient and mild in 4 patients) in 104 patients whose pancreatic juice obtained by ERP.

Diagnostic Cutoff Levels for the Tumor Size, MPD Size, Mural Nodule Size, and CEA Levels in the Pancreatic Juice for the Prediction of Malignant IPMN

In this study, ROC curves were used to determine the cutoff levels for the tumor size, MPD size, mural nodule size, and CEA level in the pancreatic juice (Fig. 1) to differentiate between benign and malignant IPMN in the patients with the branch duct type IPMN. Mathematically, the cutoff values were defined as those corresponding to points on the ROC curve situated furthest away from the reference line. The areas under curve for the tumor size, MPD size, mural nodule size, and CEA level in the pancreatic juice were 0.612, 0.711, 0.819, and 0.920, respectively, and the determined cutoff levels for the differentiation between benign and malignant IPMNs were 30 mm, 5 mm, 5 mm, and 30 ng/mL, respectively (Table 2).

TABLE 1. The Demographics and Clinical Characteristics of 134 Patients With Branch Duct Type IPMN

Characteristics	Value
Age, mean ± SD (range), yr	68.9 ± 9.7 (32–84)
Sex, male/female	74/60
Tumor size, mean ± SD (range), mm	30.4 ± 12.3 (5–88)
Main pancreatic duct size, mean ± SD (range), mm	6.5 ± 4.2 (1–20)
Mural nodule size, mean ± SD (range), mm	5.5 ± 5.0 (0–20)
Operation	
Total pancreatectomy	3 (2.2%)
Pancreatoduodenectomy (PD/PpPD/PrPD)	101(17/43/41) (75.4%)
Distal pancreatectomy	14 (10.5%)
Central pancreatectomy	16 (11.9%)
Histopathology	
Adenoma	51 (38.1%)
Borderline	5 (3.7%)
Carcinoma in situ	41 (30.6%)
Invasive IPMC	37 (27.6%)

PpPD indicates pylorus-preserving PD; PrPD, pylorus-resecting PD

© 2012 Lippincott Williams & Wilkins

Copyright © 2012 Lippincott Williams & Wilkins. Unauthorized reproduction of this article is prohibited.